JOINT INSTITUTE FOR NUCLEAR RESEARCH
Frank Laboratory of Neutron Physics

FINAL REPORT ON THE START PROGRAMME

Investigation of morphology and structural changes of lipid membranes

Supervisor:
Dr. Alexander Ivanovich Kuklin

Student:
Dmitriy Rufov, Russia
Moscow Institute of Physics and Technology

Participation period:
February 16 – March 29, Winter Session 2025

Dubna, 2025

Contents

1 Abstract

Liquid–solid phase transitions in lipid membranes play a key role in the regulation of cellular processes, including synaptic transmission, thermoregulation, and anesthesia mechanisms. These transitions are accompanied by significant changes in the physico-chemical properties of the membranes, such as surface area, thickness, and interaction with ions (for example, Ca^{2+}), which makes them critical for cell function.

This makes the study of phase transitions and morphology of lipid membranes an important part of the study of cell function. In this paper, we study model lipids (DMPC), which can provide knowledge about some characteristic processes occurring in natural systems, such as the temperature of the phase transition, the volume per lipid molecule, etc.

2 Introduction

Lipid membranes are key components of biological systems, ensuring the structural integrity of cells and participating in the most important biochemical processes. Their morphology and physico-chemical properties are determined by their phase behavior, which depends on temperature, pressure, lipid composition and other factors (Figure 1). Lipid membranes can be in various phase states, including lamellar (layered: $L_c, L_{\beta'}, L_\alpha, P_{\beta'}$) and non-lamellar (hexagonal, cubic: $Q^P_{II}, Q^G_{II}, Q^D_{II}, H_{II}$) phases. The closest to what occurs in nature are lamellar phases, such as:

L_α-phase (liquid crystal): In this phase, the lipid acyl tails are in a molten state, having high mobility, and the membrane itself is characterized by low order. This phase is biologically the most relevant, as it corresponds to the state of membranes in living cells.

$L_\beta, L_{\beta'}$-phase (gel phase): In this phase, the lipid acyl tails are ordered and elongated, forming a dense package. The membrane in this phase is less mobile and more rigid. The bar at the beta index means that the acyl chains of lipids are at an angle to the normal of the membrane.

$P_{\beta'}$-phase (ripple phase): This phase is an intermediate state between the L_β- and L_α-phases. It is characterized by periodic bends of the membrane, forming "ripples". The ripple phase is observed, for example, in dimyristoyl phosphatidylcholine (DMPC) under certain conditions and other saturated phospholipids.

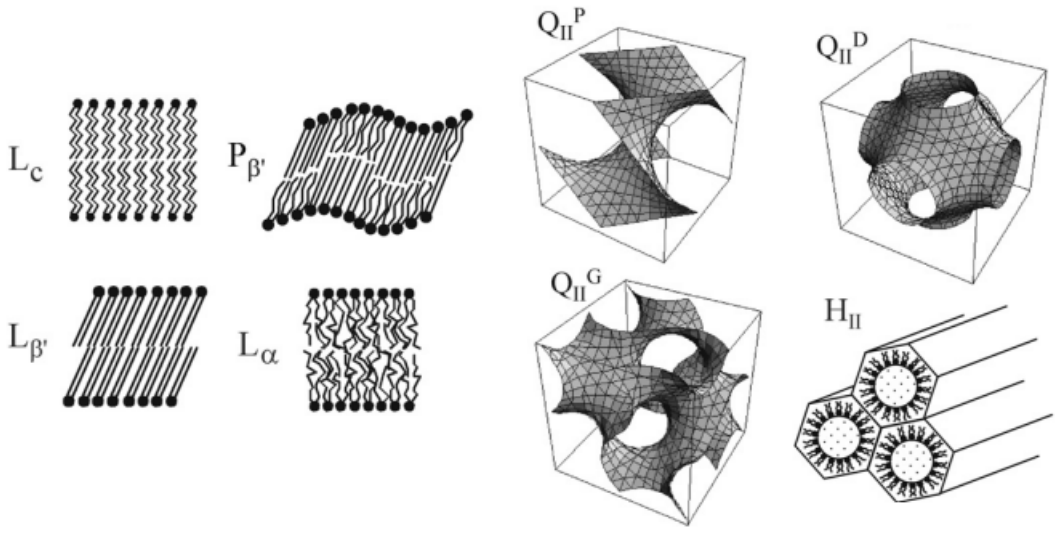

Figure 1: Schematic representation of various lipid phases characteristic of membrane lipids

The phase transition changes some parameters of lipid molecules. For example, the phase transition from the gel phase to the liquid crystal phase is accompanied by an increase in the area per lipid molecule and a decrease in the length of the acyl chains, reflecting the disordering of the hydrocarbon tails. The volume per 1 lipid molecule also changes. When switching from $L_{\beta'}$ to $L\alpha$ it increases sharply.

3 Project goals

The aim of the work was to study the change in the morphology and parameters of lipid membranes and molecules depending on various methods of preparation and solvent substances. Since most physiologically significant results should be obtained in water (H_2O), because it contains most of the cells of organisms, but the vast majority of neutron scattering experiments are carried out by dissolving lipids in heavy water D_2O. It is necessary to determine the phases characteristic of the lipid at different temperature and to determine the temperatures of phase transitions. Since DMPC is one of the important model lipids, inc behavior has been studied.

4 Materials and methods

Theoretical foundations of SANS and SAXS

The methods of small-angle neutron scattering (SANS) and X-rays (SAXS) are powerful tools for studying the structural features of substances. These methods are based on the analysis of elastic coherent scattering of radiation on inhomogeneities of matter density.

When a plane monochromatic wave with an amplitude of $A_0 \exp(i\mathbf{k_0 r})$ falls on the scattering center, a secondary scattered spherical wave arises, described by the expression:

$$A(\mathbf{r}) = A_0 \exp(i\mathbf{k_0 r}) + A_0 \frac{b}{r} \exp(i\mathbf{kr}), \tag{1}$$

where $\mathbf{k}_0$ and $\mathbf{k}$ are the wave vectors of incident and scattered waves, b is the scattering length, depending on the type of radiation and the nature of the scattering center.

The amplitude of the scattered radiation is related to the spatial distribution of the scattering density $\rho(\mathbf{r})$ by the Fourier transform:

$$A(\mathbf{q}) = \int_V \rho(\mathbf{r}) \exp(i\mathbf{qr})\, dV, \tag{2}$$

where $\mathbf{q} = \mathbf{k} - \mathbf{k}_0$ is the scattering vector, $|\mathbf{q}| = \frac{4\pi}{\lambda} \sin(\theta/2)$, λ - the wavelength of the radiation, θ is the scattering angle.

For isotropic systems, after orientation averaging, the scattering intensity depends only on the modulus $q = |\mathbf{q}|$:

$$I(q) = \langle |A(\mathbf{q})|^2 \rangle = \left\langle \left| \int_V \rho(\mathbf{r}) \exp(i\mathbf{q} \cdot \mathbf{r})\, dV \right|^2 \right\rangle. \tag{3}$$

This averaging leads to Debye's formula:

$$I(q) = \int_V \int_V \rho(\mathbf{r}) \rho(\mathbf{r}') \frac{\sin(q|\mathbf{r} - \mathbf{r}'|)}{q|\mathbf{r} - \mathbf{r}'|}\, dV\, dV'. \tag{4}$$

For q =0, the expression for the scattering intensity takes the form:

$$I(0) = \left| \int_V \rho(\mathbf{r}) dV \right|^2 = N(\Delta\rho)^2 V_p^2, \tag{5}$$

here V_p is the volume of one particle.

For a system of particles in a highly dilute solution, the scattering intensity is expressed in terms of the form factor $F(q)$ and the structural factor $S(q)$:

$$I(q) = N|F(q)|^2 S(q). \tag{6}$$

In the case where the particle interaction can be neglected, $S(q) \approx 1$.

For example, for spherical particles with a radius of R:

$$F(q) = 3V \frac{\sin(qR) - qR\cos(qR)}{(qR)^3}, \tag{7}$$

where V is the volume of the particle.

In the region of small angles ($qD < 1$, where D is the characteristic size of the particle under study), the following approximations can be used.

For globular particles (all three spatial dimensions of the same order):

$$ln\,(I(q)) = ln\,(I(0)) - \frac{q^2 R_g^2}{3}. \tag{8}$$

For highly elongated particles (one of the spatial dimensions L is much larger than the other two d_x, d_y, i.e. $L >> d_x, d_y$):

$$ln\,(qI(q)) = ln\,(I(0)) - \frac{q^2 R_c^2}{2}. \tag{9}$$

For flat particles (one of the spatial dimensions T is much smaller than the other two, d_x, d_y, i.e. $T << d_x, d_y$):

$$ln\left(q^2 I(q)\right) = ln\,(I(0)) - q^2 R_t^2. \tag{10}$$

Here R_g, R_c, R_t are the radii of inertia of the globular, the cross-section of the elongated particle, and the thickness of the flat particle, respectively.

Small-angle X-ray and neutron scattering methods provide complementary information: 1) SAXS is sensitive to the distribution of *electron density*, 2) SANS: registers scattering on *atomic nuclei*.

1) X-ray scattering occurs mainly on electrons (the contribution of nuclei is negligible, since the mass of the nucleus is about 10^3 times the mass of an electron). When scattering by a free electron, the amplitude of the scattered wave is E_s:

$$E_s = -E_0 \frac{e^2}{mc^2} \frac{1}{r} \sin\psi, \tag{11}$$

where E_0 is the amplitude of the electric field oscillations in the incident wave, e is the charge of the electron, m is its mass, c is the speed of light, r is the distance from this free electron to the observation point, *psi* is the angle between the scattered beam and the direction of acceleration of the electron.

In low-angle mode ($\psi \approx 90°$):

$$b_x = r_0 = \frac{e^2}{mc^2} \approx 2.82 \times 10^{-13} \text{ см}, \tag{12}$$

is equal to the classical radius of the electron r_0.

For an atom with Z electrons:

$$f_a = r_0 Z. \tag{13}$$

2) The wavelength of a neutron is determined by the de Broglie relation:

$$\lambda = \frac{h}{mv} \tag{14}$$

If neutrons pass through a moderator with a temperature of T, then the average square of their velocity, according to the equipartition theorem, satisfies the following expression (k_B – Boltzmann constant):

$$\frac{m\langle v^2 \rangle}{2} = \frac{3}{2} k_\text{Б} T. \tag{15}$$

In this case, the maximum in the spectrum of neuron wavelengths falls on

$$\lambda_{max} = \frac{h}{\sqrt{3mkT}} \tag{16}$$

Scattering occurs mainly on the nuclei. The scattering length depends on the isotope and spin orientation, and it can be either positive or negative. In addition, the amplitude of neutron scattering is weakly dependent on the scattering angle.

Time-of-flight equipment

Unlike monochromatic X-ray radiation with a constant wavelength, neutrons produced by a nuclear reactor are characterized by a wide spectral distribution. To accurately determine the wavelength of the detected neutrons, a principle based on measuring the duration of particle flight, called time-of-flight technique (TOF), is used.

The relationship between the wave properties of neutrons and their kinetic parameters in the non-relativistic approximation is established through the equation for their wavelength:

$$\lambda = \frac{h}{p} = \frac{h}{m_n v} = \frac{h}{m_n} \cdot \frac{t}{L} \tag{17}$$

where h is Planck's constant, m_n is the rest mass of the particle's neutron, L is the distance traveled between the source and the detector, and t is the fixed travel time.

To simplify, you can substitute constant values into the expression and get the formula:

$$\lambda[\mathring{A}] = 3.956 \cdot \frac{t\,[\text{ms}]}{L\,[\text{m}]} \tag{18}$$

As a result, in order to determine the wavelength of a neutron, it is necessary to record the time of neutron flight by the detector and know the flight base - the distance to the detector.

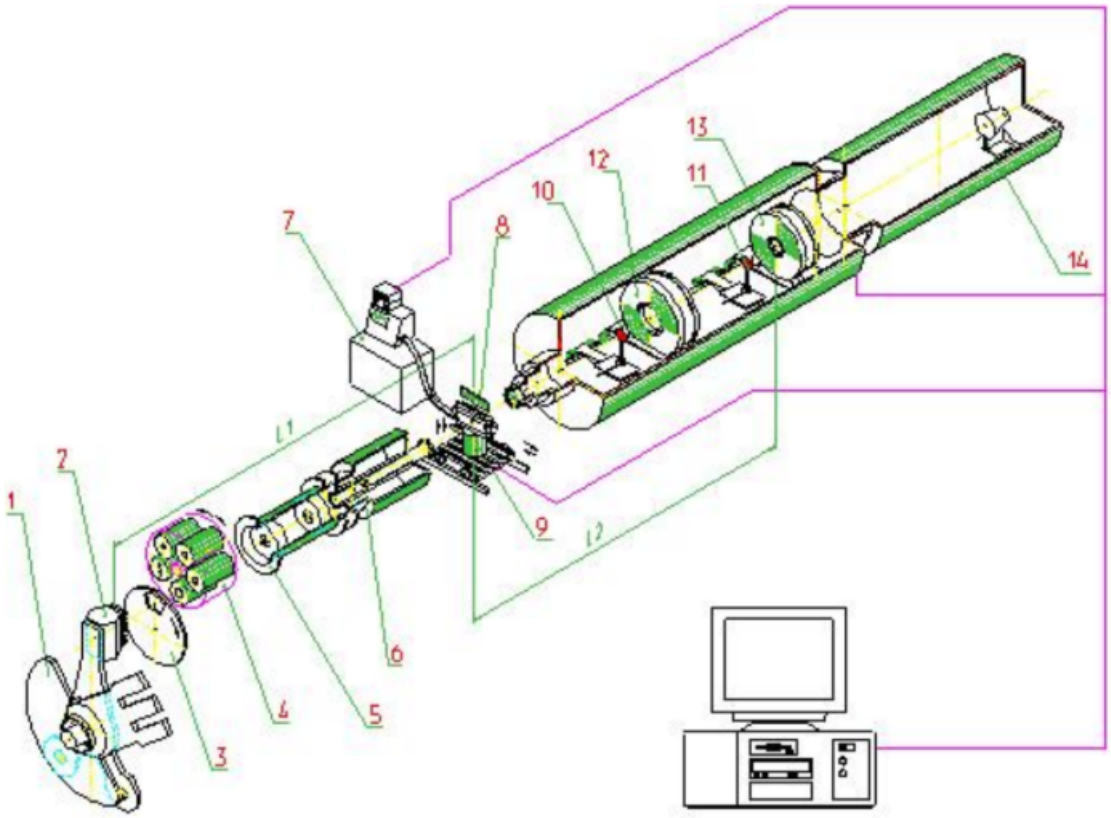

Figure 2: Diagram of the YuMO spectrometer. 1. Movable reflector. 2. An active zone with a water moderator that thermalizes the neutron flux. 3. An interrupter that suppresses the background and pulses generated by an additional reflector. 4-6. A collimator system that generates a stream of thermal neutrons. 7. A computer-controlled thermostat. 8. The test sample. 9. A sample table with a goniometric node with three degrees of freedom. The table is located in the air, which makes it easy to mount and remove additional devices. 10. Vanadium standard. Its periodic introduction and removal from the neutron beam makes it possible to avoid undesirable long-period fluctuations in the radiation power and obtain intensity values in absolute units. 11, 12. Two annular gas-filled neutron detectors («OLD» – 11 and «NEW» – 12). 13. Direct beam neutron detector.

YuMO Spectrometer

The YuMO small-angle thermal neutron scattering spectrometer is located at JINR (Dubna) on the fourth channel of the pulsed fast neutron reactor IBR-2M. Measurements on it are carried out using time-of-flight technology (TOF). The description and diagram of the installation with its main elements is shown in the figure 2.

The experimental facility for studying small-angle neutron scattering includes detectors placed in a vacuum chamber on special mobile platforms. These detectors can move along the axis of the neutron beam at a distance of about 10 meters, which makes it possible to optimally adjust the geometry of the experiment by adjusting the distances from the sample to each of the detectors.

Vanadium standards are an important part of the spectrometer, the geometric dimensions and location of which are carefully selected. They are positioned in such a way as to register only a direct neutron beam, excluding the influence of scattered radiation. This ensures the accuracy of calibration measurements.

The experiment is conducted in two stages. First, the sample is placed in a neutron stream

with vanadium standards set aside. Then the second stage is performed, when both the sample and the standards are under a neutron beam together. This technique allows for absolute neutron scattering calibration.

To increase the accuracy of measurements, the calibration procedure is repeated at regular intervals. This makes it possible to compensate for possible long-term fluctuations in reactor power and avoid additional errors.

Densimetry

The Anton Paar DMA 5000M density meter is based on the principle of measuring the resonant frequency of a U-shaped oscillating tube (рис. 3) f filled with the liquid under study. This method is one of the most accurate and widely used in industry and scientific research for measuring the density of liquids.

Figure 3: U-shaped tube of the densimeter

The vibrations of the tube are excited by an alternating electromagnetic field, which creates a periodic force that varies according to a harmonic law. This force "rocks" the tube, causing it to move from side to side, and the Anton Paar DMA 5000 density meter specifically adjusts the excitation frequency to the resonant frequency of the tube (at which the amplitude of its oscillations is maximum). The resonance effect increases the accuracy and allows you to calculate the density in this implementation up to 6 decimal places.

The equation of harmonic vibrations of a tube:

$$(m + m_s)\frac{d^2x}{dt^2} + kx = Fcos(\omega t),$$

where m is the mass of the tube, m_s is the mass of the sample, x is the deviation of the tube from the equilibrium position, k is the stiffness coefficient of the tube, F is the amplitude of the driving force, ω is the circular frequency of the driving force.

Resonance occurs when the frequency of the driving force is equal to the natural oscillation frequency of the tube $\omega_0 = \sqrt{\frac{m+m_s}{k}}$, i.e. in the case of $\omega = \omega_0$.

Then the oscillation frequency $f = 2\pi\omega = 2\pi\sqrt{\frac{m+m_s}{k}}$.

Writing the formula for the mass of the sample in terms of its density ρ_s and the volume that the tube V contains, and expressing the sample density from the resulting equation, we have

$$\rho_s = \frac{k}{4\pi^2 V}f^2 - \frac{m}{V}.$$

It is not difficult to see that the desired density is expressed in terms of the measured frequency as $\rho_s = Af^2 - B$, where A, B are some constants of the device. Calibration on air and water of known densities allows us to calculate these constants, which allows us to further use the density meter to measure the densities of other samples.

Density measurement range: $0 - 3\,\mathrm{g/cm^3}$.
Density measurement accuracy: $5 \times 10^{-6}\,\mathrm{g/cm^3}$.
Temperature measurement range: $0 - 95\,℃$.
Temperature measurement accuracy: $0.01\,℃$.
Minimum sample volume: 1 ml.

The image of this ANTON PAAR 5000M density meter is shown in the figure 4.

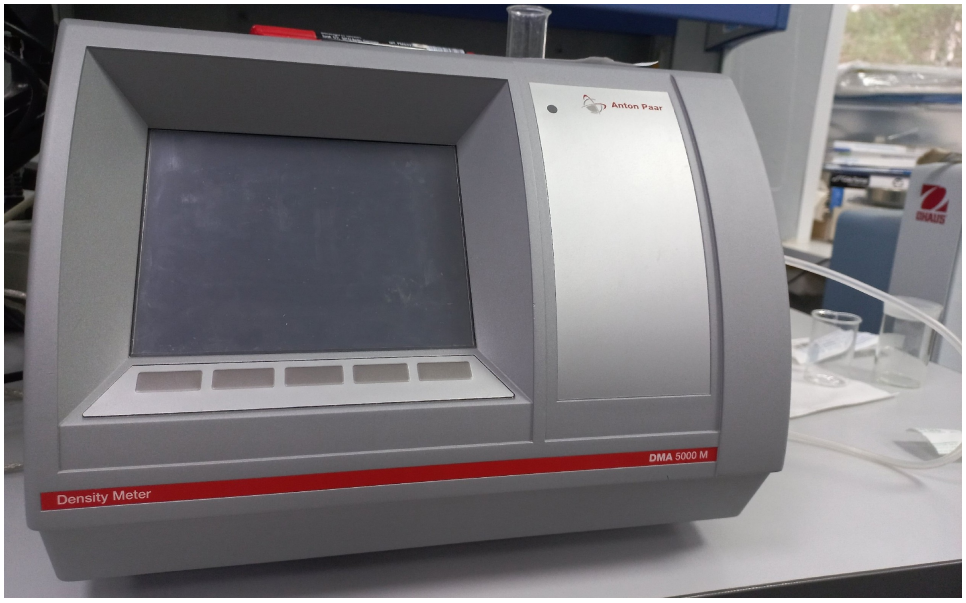

Figure 4: ANTON PAAR 5000M density meter

Preparation of lipid by extrusion

To prepare the lipid by extrusion, it was mixed with a solvent (H_2O or D_2O) in the required proportions. Then the resulting mixture was placed in a compact thermomixer for 2 minutes at a speed of 900 rpm. Then, using an extruder, it was passed through filters with pores of 50 nm 11 times.

Preparation of lipid by ultrasound

To prepare the lipid using ultrasound, it was mixed with a solvent (H_2O or D_2O) in the required proportions. The resulting mixture was then placed under ultrasound for 10 minutes.

Degassing

Degassing of the samples was performed as follows. A magnetic stirrer was placed in the sample. The sample was placed on a magnetic table, which rotated the magnetic stirrer at a speed of 1200 rpm. Then the sample was covered with a hood, from under which air was pumped out. The degassing itself lasted 15 minutes.

5 Results

Samples of DMPC lipid were prepared in solutions of water H_2O and heavy water D_2O in a lipid/water mass ratio of 1% or 0.5% using ultrasound or extrusion, since these methods make it possible to obtain single-layer vesicles. Next, all samples were degassed to eliminate the influence of air on the final results. After preparation, the dependence of the sample density and volume per 1 lipid molecule on temperature was determined. The results are shown in the pictures 5 and 6.

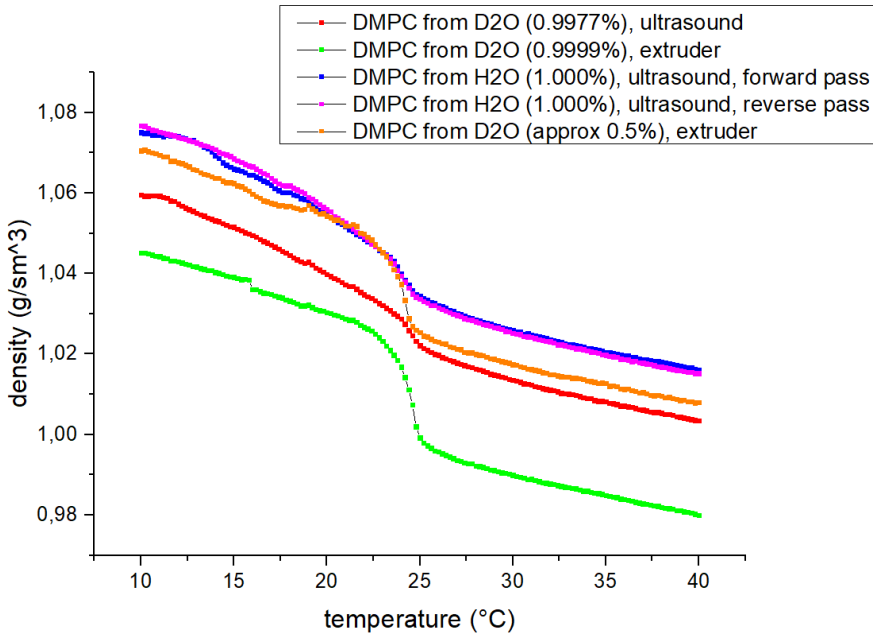

Figure 5: Temperature dependence of the density of various DMPC lipid samples.

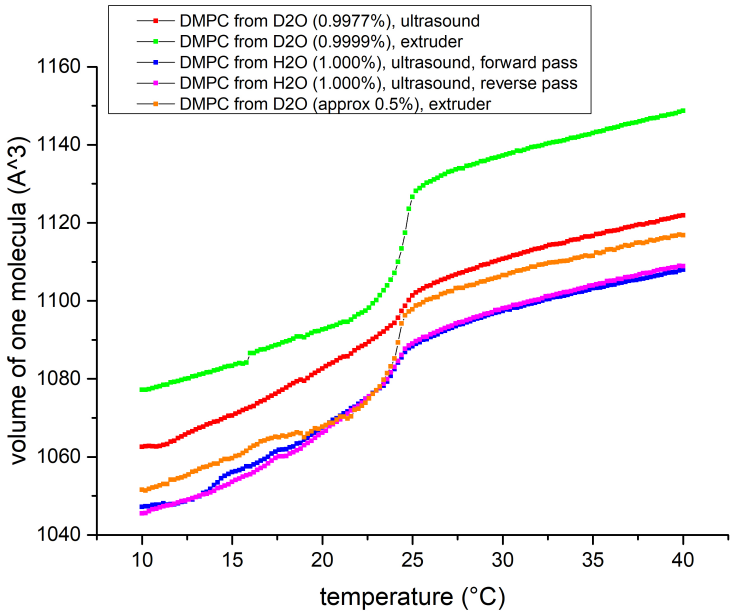

Figure 6: Temperature dependence of the volume of one DMPC lipid molecule.

It can be seen from these graphs that the method of preparation affects the dependence of the density of a lipid and the volume of one of its molecules on temperature. For example,

samples that were prepared by extrusion experience a significant jump in both density and volume near the temperature of the main phase transition (about 24 ℃), while samples that were prepared using ultrasound show a much smaller jump. Also, the feed obtained using an extruder can be observed transitioning to the ripple phase in the region of 15 ℃, which is especially well demonstrated by the green graph (DMPC dissolved in heavy water in a mass ratio of 1%, prepared by extrusion). Additionally, for an aqueous (H_2O), i.e., a physiologically significant sample, a density meter was measured both in the forward direction (to increase the temperature) and in the reverse direction (to decrease). It can be seen that there are practically no changes in the course of the curves (blue and magenta).

The first derivative was calculated for all curves of the volume versus temperature. The received data is shown in the picture 7 (a-e).

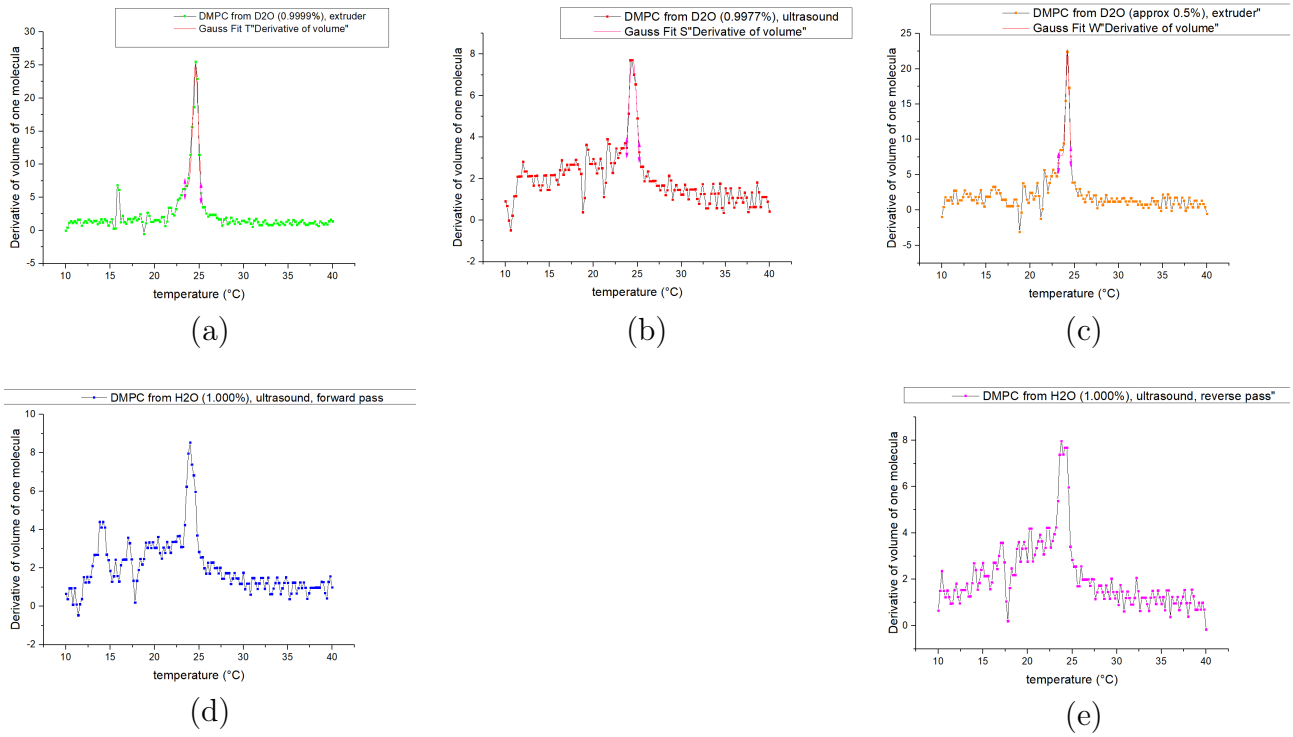

Figure 7: Graphs of derived densities of the studied DMPC samples

It can be seen that each curve has a characteristic peak, which corresponds to a jump in the volume graph, or a break in the derivative. We find the position of the center of its peak, which characterizes the temperature of the main phase transition and the peak width (Table 1).

Table 1. Temperatures of the main phase transition for various DMPC samples

Sample	T_c, °C	ΔT_c, °C	w, °C	Δw, °C
D_2O, ultrasound, 0.9977%	24.47	0.03	1.2	0.7
D_2O, extruder, 0.9999%	24.58	0.03	0.58	0.09
H_2O, ultrasound, 1.000%, forward pass	24.05	0.02	1.3	0.5
H_2O, ultrasound, 1.000%, reverse pass	23.99	0.04	1.00	0.17
D_2O, extruder, approx 0.5%, extruder	24.211	0.017	0.37	0.04

It can be seen that the temperature of the main phase transition in D_2O is slightly higher than in H_2O.

Also, some graphs (a, d) show a characteristic peak, which apparently corresponds to the transition from the gel to the ripple phase.

To analyze the structure of lipid membranes, a sample of 3.5% DMPC solution in D_2O was prepared by extrusion through 200 nm pores and studied by small-angle neutron scattering. The data on this scattering is shown in the figure 8.

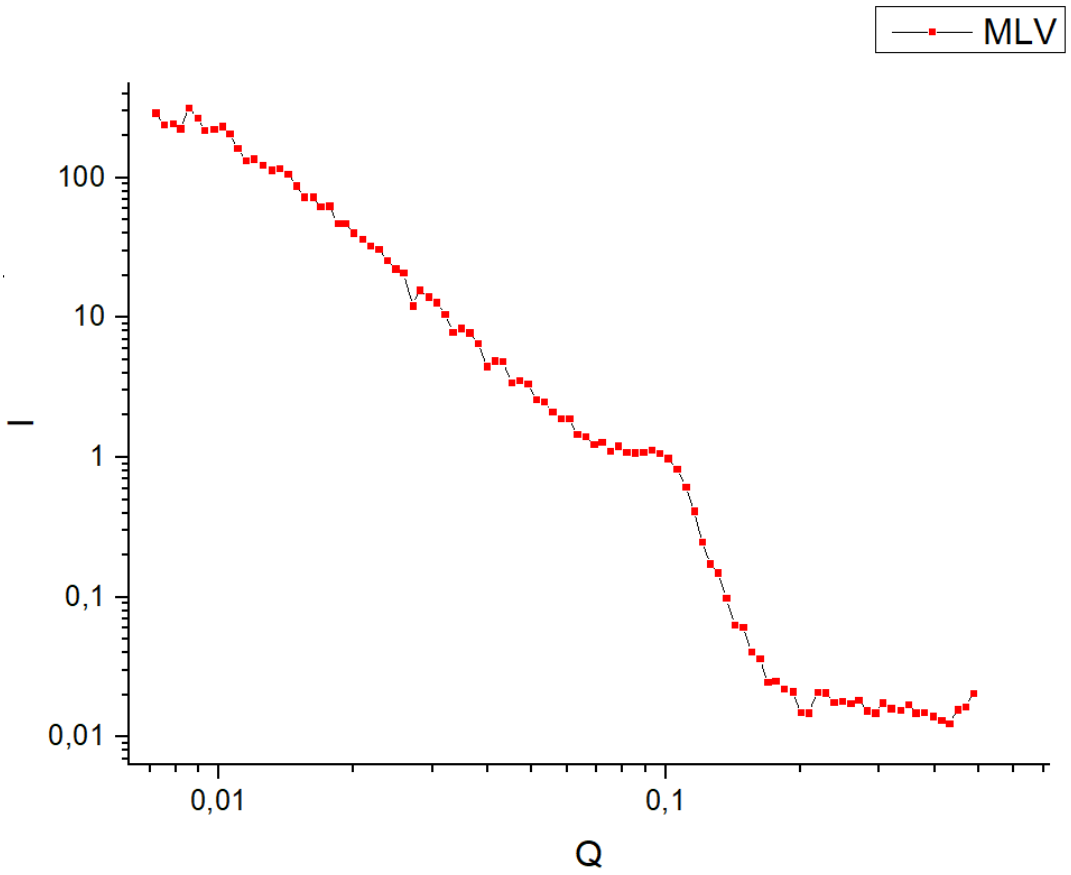

Figure 8: Dependence of the scattering intensity I on the scattering vector Q.

It follows from the graph that with this lipid ratio and the preparation method, the morphology of the resulting sample is multilayer vesicles (MLV). This conclusion is made from the diffraction peak obtained at $q = 0.097\ \mathring{A}^{-1}$, which is recalculated into the distance between the vesicle layers according to $d = \frac{2\pi}{q}$. Then the resulting distance between the layers of multilayer vesicles is: $d \approx 65\ \mathring{A}$.

6 Conclusion

The work investigated the effect of the preparation of lipid solutions and the solvent itself on the morphology, properties of lipid membranes and characteristics of their phase transitions.

It was found that the temperature of the main phase transition of DMPC solutions depends on which water it was dissolved in (D_2O or H_2O). It turned out that this temperature is slightly higher in D_2O. This may mean that heavy water is able to better structure the lipid membrane, which helps to reduce its randomness (entropy), which makes it difficult to transition to the liquid crystal L_α-phase.

To study the morphology, the method of small-angle neutron scattering was applied, which allowed us to determine that the extruded through 200 nm pores in the ratio of lipid/water 3.5% DMPC sample forms multi-layered vesicles with a distance between the layers $d \approx 65$ Å.

7 References

[1] Овчинников Ю.А. Биоорганическая химия. Рипол Классик, 1987.

[2] Геннис Р. Биомембраны: Молекулярная структура и функции. М.: Мир, 1997.

[3] R. Winter and C. Jeworrek, *Effect of pressure on membranes*, Soft Matter, 2009, **5**, 3157–3173. DOI: https://doi.org/10.1039/b901690b10.1039/b901690b.

[4] R. Winter and W.-C. Pilgrim, *A SANS Study of High Pressure Phase Transitions in Model Biomembranes*, Berichte der Bunsengesellschaft für physikalische Chemie, 1989, **93**, 708–717. DOI: https://doi.org/10.1002/bbpc.1989093060610.1002/bbpc.19890930606.

[5] A. G. Soloviev et al., *SAS program for two-detector system: seamless curve from both detectors*, Journal of Physics: Conference Series, 2017, **848**, 012020. DOI: https://doi.org/10.1088/1742-6596/848/1/01202010.1088/1742-6596/848/1/012020.

[6] Харакоз Д. П. *О возможной физиологической роли фазового перехода «жидкое–твердое» в биологических мембранах* // Успехи биологической химии. — 2001. — Т. 41. — С. 333—364.

[7] Anton Paar GmbH, *DMA 5000 Density Meter - User Manual*, User manual, Version 1.0, Anton Paar, 2021.

[8] Свергун Д.И., Фейгин Л.А. Рентгеновское и нейтронное малоугловое рассеяние. Наука. Гл. ред. физ.-мат. лит., 1986.